

# Evaporation-driven generic, high-throughput and roll-to-roll printing of nanomaterials

Received: 21 November 2024

Accepted: 8 November 2025

Published online: 10 December 2025

Check for updates

Xu Xiang<sup>1,5</sup> , Jia-Hui Xin<sup>2,3,5</sup>, Yu-Wei Liu<sup>1,2,5</sup>, Chao Zhang<sup>2,3</sup> , Zhi-Han Liu<sup>1</sup>, Hai-Yun Ou<sup>1</sup>, Hai-Feng Zhang<sup>1</sup>, Chao Zheng<sup>1</sup>, Chun-Wen Guo<sup>1</sup>, Xiao-Bing He<sup>4</sup>, Hao-Cheng Yang<sup>2,3</sup> & Zhi-Kang Xu<sup>2,3</sup>

Manufacturing low-dimensional nanomaterials into macroscopic films, going beyond the limit of conventional polymer counterparts, can unleash the potential of advanced separation, energy harvesting, optical/thermal management, and soft robotics. Despite enormous achievements, it remains untouchable to achieve large-scale and high-throughput manufacturing of arbitrary nanomaterials into uniform films using a facile and generic strategy. Herein, we demonstrate an original evaporation-driven printing (EDP) approach that enables high-throughput roll-to-roll and spatially-programmable fabrication of various nanomaterials into multi-functional composite films, overcoming the limitations of conventional strategies demanding specific physicochemical properties of nanomaterials. The EDP approach leverages a ubiquitous physical phenomenon of water evaporation for driving rapid bottom-up mobility and gathering of nanomaterials toward the evaporated interface and eventually assembling into orientated nanomaterial-stacked films on the surface of porous substrates due to the presence of size-screening effect. Unlike conventional nanomaterials printing, the EDP can be applicable for arbitrary nanomaterials from 2D nanosheets to 1D nanotube and their combination for multi-materials and recyclable printing without the need of extra additives. EDP-manufactured graphene oxide films can be harnessed as desalination with over 95.0% rejection for sodium sulfate, outperforming most graphene oxide-based counterparts. Moreover, EDP is also capable of printing high-performance electromagnetic shielding materials by virtue of printed ordered lamellar structures as continuous conductive pathways.

Low-dimensional nanomaterials possessing intriguing physicochemical properties over their bulky ones have been routinely recognized as promising building blocks to manufacture functional films that go beyond conventional polymer counterparts<sup>1–3</sup>. Particularly, 2D

nanosheets have emerged as benchmark candidates to fabricate nanosheet-stacked lamellar films, exhibiting enormous potential in the fields of advanced separation<sup>4–6</sup>, energy harvesting<sup>7–9</sup>, optical/thermal management<sup>10,11</sup>, and soft robotics<sup>12</sup>. Powered by these unique traits, a

<sup>1</sup>School of Materials Science and Engineering, Chongqing Jiaotong University, Chongqing, China. <sup>2</sup>MOE Key Lab of Macromolecular Synthesis and Functionalization, Department of Polymer Science and Engineering, Zhejiang University, Hangzhou, China. <sup>3</sup>The “Belt and Road” Sino-Portugal Joint Lab on Advanced Materials, International Research Center for X Polymers, Zhejiang University, Hangzhou, China. <sup>4</sup>School of Civil Engineering, Chongqing Jiaotong University, Chongqing, China. <sup>5</sup>These authors contributed equally: Xu Xiang, Jia-Hui Xin, Yu-Wei Liu. e-mail: [xxiang1984@cqjtu.edu.cn](mailto:xxiang1984@cqjtu.edu.cn); [zhangchao7@zju.edu.cn](mailto:zhangchao7@zju.edu.cn); [xuzk@zju.edu.cn](mailto:xuzk@zju.edu.cn)

series of 2D nanosheets has been synthesized by both top-down and bottom-up approaches over the past decade, primarily including graphene oxide (GO), MXene, MoS<sub>2</sub>, BN, Metal-Organic Framework (MOF) and Covalent Organic Framework (COF). However, the key challenge of this field lies in how to manufacture these 2D nanosheets into intact lamellar films at a large scale<sup>13,14</sup>. The current mainstream manufacturing methods mainly include vacuum filtration/spin/blade-assisted assembly<sup>15–18</sup>, interfacial self-assembly<sup>19–21</sup> and inkjet/direct-ink-write (DIW) printing<sup>22–24</sup>. Despite great success in the above-mentioned assembly strategies, it remains challenging to construct large-scale, high-quality nanosheet-stacked lamellar films, as imposed by the susceptible and uncontrollable assembly process at a large scale, especially for the distinct physicochemical properties of various nanomaterials. For inkjet and DIW printing, they normally necessitate specific rheological properties of nanomaterial dispersion by introducing functional additives and suffer from an undesirable dot/line-scan mode with a low printing rate, markedly restricting further application<sup>25–27</sup>. To this end, it is exigent to develop a facile, generic and high-throughput strategy to manufacture arbitrary nanomaterials into large-scale and uniform films.

Water evaporation, characterized by a physical phase change process from liquid to vapor, is an omnipresent phenomenon in nature and has been heavily investigated and applied in a myriad of fields such as energy, environment, and nanofluidic<sup>28</sup>. When water molecules are evaporated from the solution, there normally exists an evaporation-induced flow phenomenon. We hypothesize that this evaporation-induced flow may be harnessed as a driving force of the directional movement of nanomaterials toward the evaporated interface. Herein, we report a facile evaporation-driven printing (EDP) of various nanomaterials on the surface of porous substrates, allowing for attaining high-throughput roll-to-roll fabrication of functional films. In the EDP process, the porous substrates were floated on the surface of nanomaterial dispersions. As water molecules move due to evaporation, nanomaterials within dispersions can be driven for rapid mobility and gathering toward the floated porous substrates, leading to the formation of orientated nanomaterial-stacked films. Distinct from conventional nanomaterial printing, the EDP is imparted with a high-throughput feature via a layer-by-layer method rather than a dot or line scan. Moreover, the EDP exhibits profound universality for arbitrary nanomaterials from 2D to 1D without the need of extra additives, as well as features some promising merits of multi-materials, recyclable, and material-saving printing. As proof of demonstration, we successfully fabricated meter-scale graphene oxide (GO) films with highly oriented structures via EDP for desalination applications, achieving a rejection rate of 96% and a water permeability of 4.3 L m<sup>-2</sup> h<sup>-1</sup> bar<sup>-1</sup>. Furthermore, the GO films annealed at high temperatures exhibited superior electromagnetic interference shielding performance (55–107 dB), exceeding conventional counterparts. Integrated with the easy manufacturing toolkit and versatile material building blocks, the EDP method offers additional flexibility and dimension in the design and application of functional nanomaterial-based films.

## Results

### Design concept and feasibility of EDP

The key to effective EDP lies in the directional driving and gathering of nanomaterials from the solution to the surface of the floated porous substrate. To achieve this, the dispersion ink containing the nanomaterials is easily subjected to a controlled heating, from which a roll-to-roll apparatus can be designed for achieving large-scale and continuous mass-production EDP (Fig. 1a, b). The heating process can induce rapid evaporation of water at the interface. This, in turn, generates a corresponding water flow that drives the movement of nanomaterials beneath the porous substrate (Fig. 1c). Meanwhile, due to the presence of a temperature difference between the evaporated surface and bulk solution, there exists a convection that introduces

shear flow beneath the substrate membrane. The local flow direction of the water near the substrate is predominantly parallel to the air-water interface. This characteristic enables it to effectively control the orientation of materials such as GO<sup>29</sup>. In combined with the porous substrate-regulated immobilization via the size-screening effect, the nanomaterials would be uniformly and stably printed on the surface of the porous substrate. The whole process involves no chemical interactions, thus eliminating the need for specific chemical compositions and additives of nanomaterials and laying the foundation for outstanding versatility and broad applicability of EDP. Compared to traditional evaporation-induced assembly and interfacial self-assembly, EDP also offers the advantage of broadening the range of applicable nanomaterials while enabling the fabrication of large-scale uniform films (Supplementary Table 1). Most importantly, with the involvement of the porous substrates, EDP enables roll-to-roll technology (Supplementary Fig. 1, Supplementary Videos 1–3), making it possible to achieve large-scale manufacturing of nanomaterial stacked films, even at meter-scale sizes, a challenging task for vacuum filtration, spin-coating, or blade-assisted assembly strategies (Fig. 1d).

To validate the feasibility of EDP, we investigated the role of evaporation with fluorescent polystyrene spheres as a sensitive indicator in this process using dense and porous substrates as contrast. As illustrated in Fig. 2a, when a dense substrate is used, there is no fluorescence observed on the substrate within 30 min, indicating the failure of EDP because dense substrates block the evaporation pathways and lead to the absence of evaporation-induced driving force. To further confirm the critical role of evaporation, we designed a series of experiments to block the evaporation pathway and obtained the same results (Supplementary Figs. 2, 3). In contrast, when a porous substrate is used, the fluorescence gradually becomes apparent within 30 min, demonstrating the gathering of fluorescent polystyrene spheres onto the substrate in the presence of evaporation (Fig. 2b). Moreover, this EDP approach can be highly suitable for various porous substrates even with different chemical compositions and pore sizes (Supplementary Figs. 4, 5), implying profound feasibility and robustness of EDP.

The evaporation-induced driving force during EDP can be further reflected by examining the stability of the as-printed nanomaterials when removing the evaporation process. For ease of observation, we selected GO as a typical example, because GO nanosheets have a natural tendency to disperse and remain suspended in water<sup>30</sup>. We found the EDP-enabled GO films can sustain structural stability without GO delamination even under long-term operation when placed in an open system accompanied by an evaporation process at 80 °C (Supplementary Fig. 6, Supplementary Video 4). In striking contrast, in a closed system saturated with water vapor, the evaporation process would be blocked, and therefore the GO films suffer from an obvious delamination of GO nanosheets into the solution, resulting in severe structural damage of the GO films. It indicates that this evaporation-induced flow is capable of serving as the driving force of nanomaterials assembly as well as maintaining the structural stability of the EDP-enabled nanomaterials-based films.

### Controllability and mechanism of EDP

The evaporation-driven nanomaterial assembly during EDP can be further manifested by orchestrating the evaporation region in porous substrates. Obviously, nanomaterials will only be assembled into the evaporation region, rather than the evaporation-blocked region. Guided by this evaporation-driven selective assembly, the EDP exhibits great capability in spatial controllability for attaining spatially programmable printing and manufacturing through the easy regulation of the evaporation region. As shown in Fig. 2c, when adding a mask onto the back of the porous substrate (termed as Back-masking, gas-phase side, Supplementary Fig. 7a) to selectively block the previous evaporation region, the nanomaterials can be shaped into various

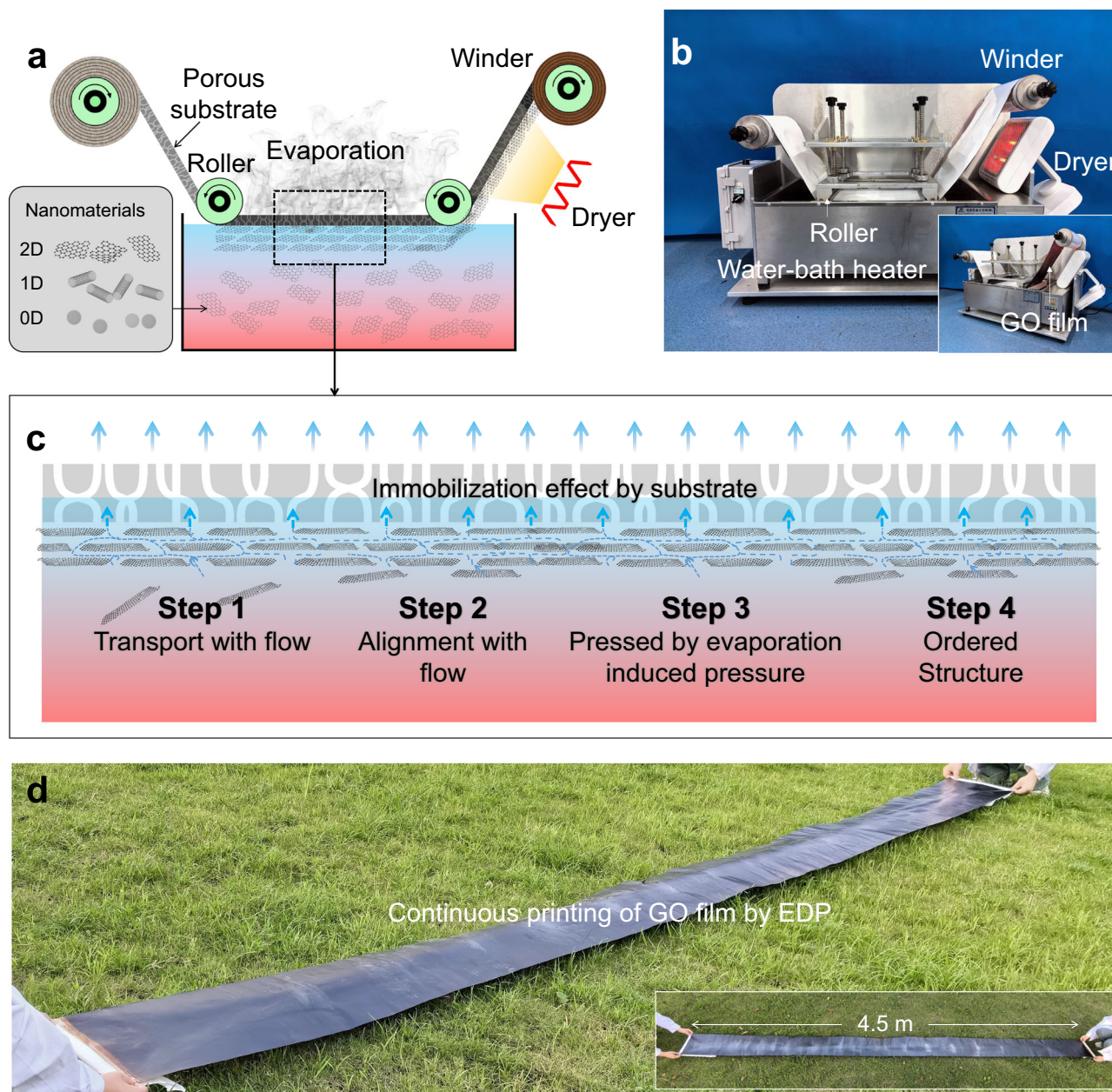


**Fig. 1 | Design concept and merits of evaporation-driven printing (EDP).**

**a** Schematic diagram of the evaporation-driven roll-to-roll printing of various nanomaterials. **b** Digital image of the evaporation-driven roll-to-roll printing apparatus. **c** Schematic diagram of the EDP process to show the role of evaporation-

induced pressure and convection in the assembly and alignment of nanomaterials. **d** Demonstration of large-scale nanomaterials-stacked films via EDP. Here, graphene oxide (GO) nanosheets were selected as a typical nanomaterial, and the EDP-enabled GO films can achieve several meters in length.

patterns, such as a horse and swallow. This selective evaporation strategy can also be reflected by adding a mask onto the front of the porous substrate (termed as Front-masking, liquid-phase side, Supplementary Fig. 7b). Analogously, a myriad of patterns can also be manufactured with high resolution (Supplementary Fig. 8). Intriguingly, with the precise and selective control over the printing region, the EDP can be endowed with the function of repaired printing, as evidenced by the repaired conductive circuit pattern that performs identically to its original state (Supplementary Fig. 9).

To quantify the utility of evaporation-induced driving force, we examined the impact of evaporation flux on the thickness of EDP-enabled films. Here, the evaporation flux during the printing process is positively correlated with the driving force according to Darcy's law (Supplementary Fig. 10)<sup>31</sup>. Fig. 2d illustrates the relationship between printing thickness and evaporation flux by taking GO as a model

nanomaterial. As the evaporation flux increases, the EDP-enabled film thickness has an obvious increase, and its slope can be used to reflect the printing rate. Consequently, an increase in evaporation flux results in a greater increment in printing thickness over the same time interval. It is noteworthy that during the EDP process, the formed film remains wet with a relatively loose internal structure, which does not hinder the evaporation of water molecules (Supplementary Fig. 11). Therefore, during the printing process, the printing rate does not decrease with the thickness increase of printed GO films, holding the potential in regulating the thickness of printed GO films with a broad range, which is different from that of vacuum filtration method. Additionally, the concentration of GO also plays a crucial role in modulating the printing rate. As demonstrated in Fig. 2e, higher GO concentrations facilitate a more rapid increase in film thickness. Notably, when both evaporation flux and GO concentration are held

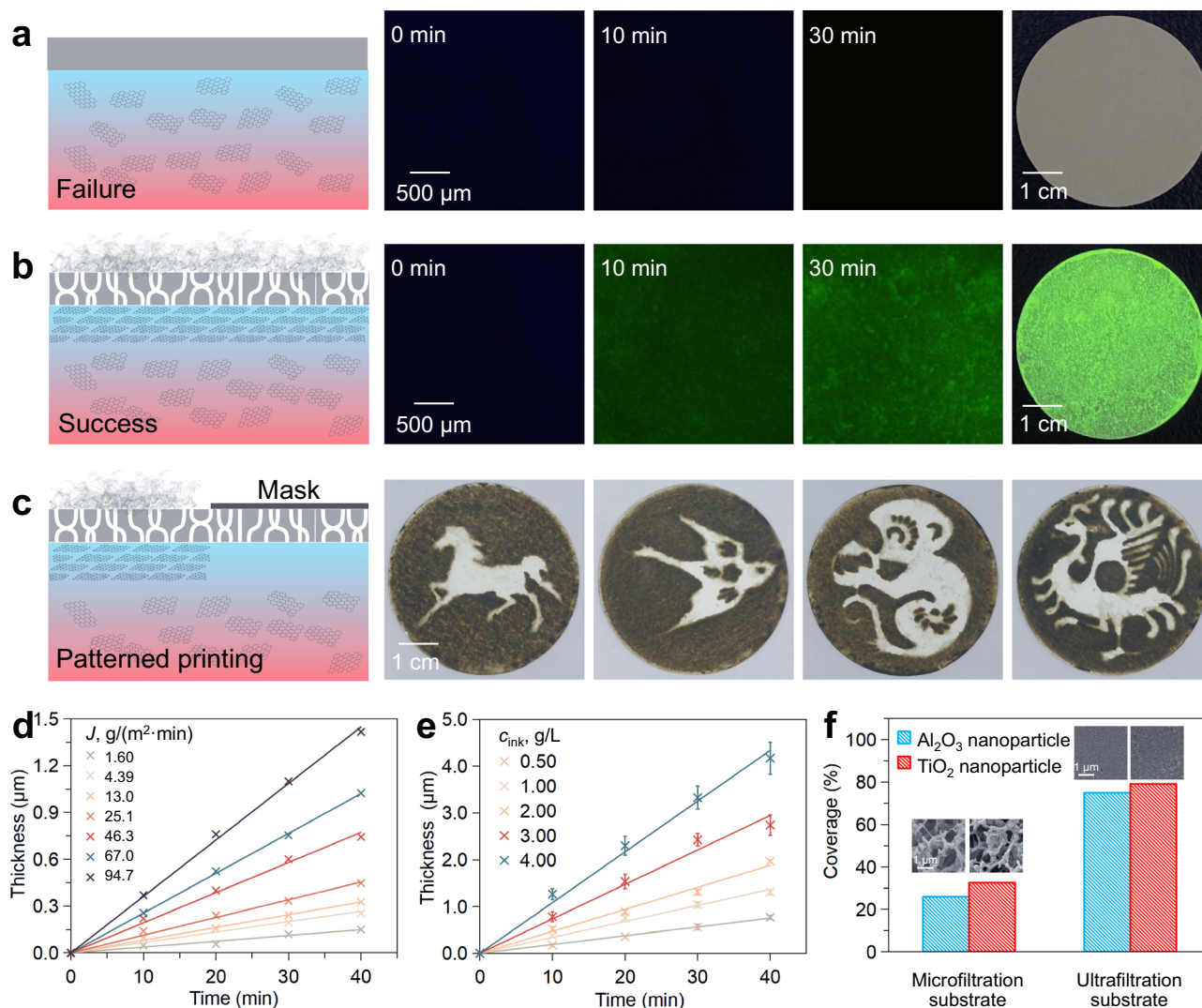


**Fig. 2 | Controllability and mechanism of EDP. a** Process evolution of EDP on a dense substrate using fluorescent polystyrene spheres as a sensitive indicator. **b** Process evolution of EDP on a porous substrate using fluorescent polystyrene spheres as a sensitive indicator. Compared with dense substrates, porous substrates can work for EDP due to the presence of evaporation. **c** Spatial

controllability of EDP by regulating the evaporation area. **d** Relationship between the thickness of EDP-enabled films and evaporation flux. **e** Relationship between the thickness of EDP-enabled films and nanomaterial concentrations. Data presented as mean  $\pm$  SD,  $n = 3$ . **f** Coverage of nanoparticles on substrate membranes with different pore sizes.

constant, the thickness increases uniformly, indicating that almost all the nanomaterials corresponding to the evaporated water portion have been successfully printed onto the substrate. Therefore, we conclude that the film thickness  $D$  can be dictated by evaporation flux and time as well as ink concentration, as shown in the following empirical equation (Supplementary Fig. 12):

$$D = \alpha J t c_{ink} \quad (1)$$

where  $J$  is evaporation flux,  $t$  is printing time, and  $c_{ink}$  is ink concentration (Supplementary Figs. 13–16, Supplementary Table 2). By fitting experimental data, the value of  $\alpha$  can be calculated to be  $0.00046 \pm 0.00005$  (Supplementary Table 3). Therefore, EDP can be used to precisely control the film thickness with linear change by easily regulating the printing process.

Apart from evaporation, the pore size of substrates also plays an important role during EDP. Porous substrates can harness their size-exclusion ability to block and fix the approaching nanomaterials during the EDP process. Briefly, when the pore size of substrates is much larger than that of nanomaterials, a majority of nanomaterials would

enter into the porous substrates rather than staying on the surface of the porous substrates. Fig. 2f shows the coverage of nanomaterials on the surface of the substrate membrane with different pore sizes. When microfiltration membranes are used as the substrate for printing metal oxide particles with small sizes, the particles enter into the pores of the substrate, resulting in a low coverage. While ultrafiltration membranes with a pore size around 8 nm are used, the coverage exceeds 70%, approaching the space utilization rate of the close packing.

Guided by the utility of the evaporation process and porous substrates, the mechanism of EDP can be understood from the following aspects. As water evaporates from the surface of the porous substrate, a continuous supply of water containing nanomaterials is drawn from the bulk dispersion due to the capillary effect. This water flow generates a pressure difference that facilitates the assembly of nanomaterials onto the substrate (Fig. 1c). The porous substrates leverage their size exclusion effect to block and immobilize approaching nanomaterials during the EDP process. Furthermore, as evaporation occurs, heat is dissipated through this process, resulting in a reduction in surface temperature and subsequently inducing convection inside dispersion driven by the temperature gradient

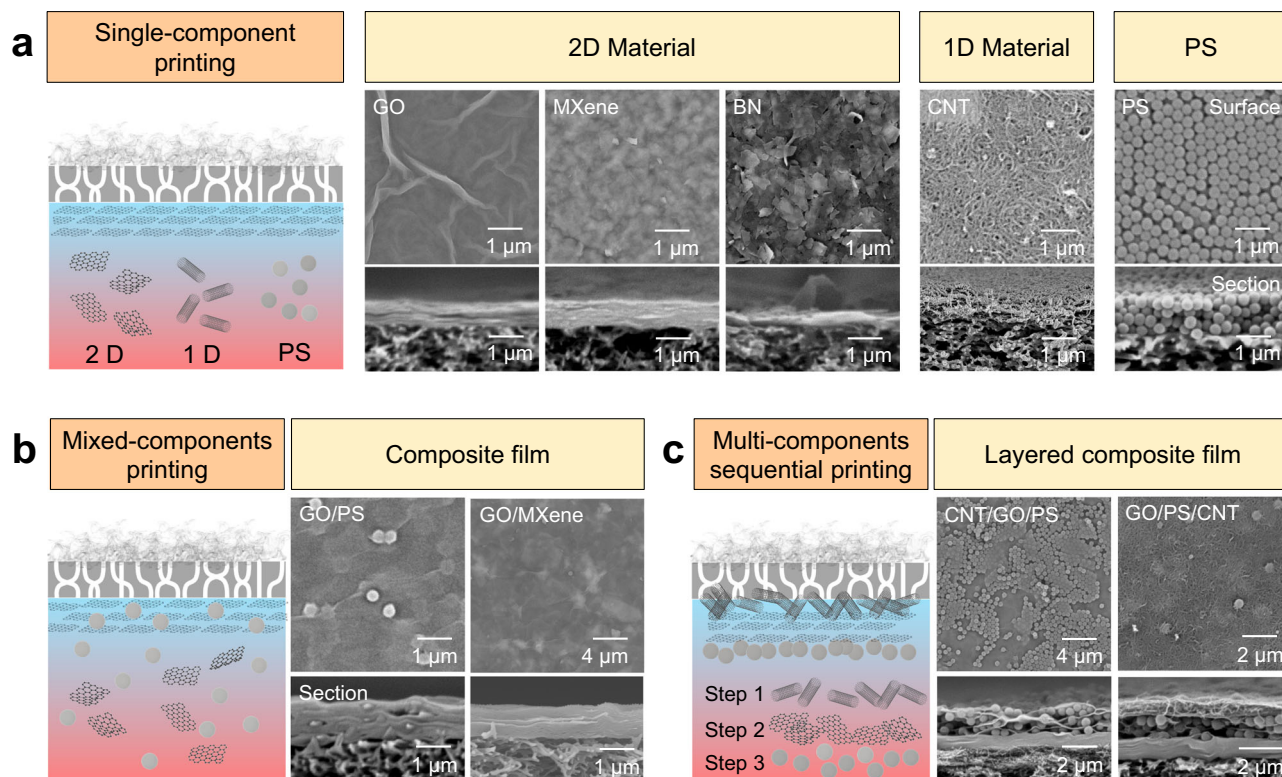


**Fig. 3 | Universality and multi-material printing of EDP.** **a** Single-component printing of 2D nanomaterials (GO, MXene, and BN), 1D nanomaterial (CNT), and PS microspheres using the EDP method. **b** Multi-material printing of EDP using a mixture of GO/PS or GO/MXene for fabricating mixed composite films. The inset

image is the distribution of the Ti element across the film (shown in yellow). **c** Multi-material sequential printing of layered composite films (CNT/GO/PS and GO/PS/CNT) using the EDP method.

(Supplementary Videos 5–7). Here, we employed Particle Image Velocimetry (PIV) for in-situ flow field analysis. By using a high-precision camera to record the motion trajectories of tracer particles, we observed that the local flow direction of water near the interface is predominantly parallel to the gas-liquid interface (Supplementary Fig. 17). The shear force generated by this parallel flow facilitates the parallel alignment of nanomaterials, such as GO, along the interface. The printing process of GO at the interface is the outcome of the combined action of local parallel flow and evaporation-driven pressure difference, with the latter one playing a dominant role. According to previous studies, the combined action of forces parallel and perpendicular to the substrate can achieve well-ordered alignment of nanosheets, with superior orientation performance compared to the effect of a single force<sup>32</sup>. Besides, the convection replenishes the nanomaterials from the bulk dispersion to the surface. This ensures a uniform distribution of nanomaterials throughout the dispersion. Thereby, the EDP method has a unique mechanism by coupling evaporation-induced mobility, alignment and assembly with the porous substrate-regulated immobilization via the size-screening effect.

### Universality and multi-material printing of EDP

Distinct from the conventional strategies demanding specific physicochemical properties of nanomaterials, the EDP is imparted with outstanding universality and can be suitable for diverse nanomaterials for precisely manipulating the composition and structure of printed films. We first studied the single-component printing of diverse nanomaterials using EDP. As illustrated in Fig. 3a, Supplementary Fig. 18, EDP excels at printing a wide range of nanomaterials, including 2D GO, MXene, Boron nitride (BN), 1D carbon nanotubes (CNT), and large-sized materials such as polystyrene microspheres (PS). Furthermore, as shown in Supplementary Fig. 19, EDP has also successfully demonstrated the printing of natural fibers (bacterial cellulose),

natural minerals (montmorillonite, kaolin), and metal oxides ( $\text{TiO}_2$ ,  $\text{Al}_2\text{O}_3$ ). The universal printing of these nanomaterials can be further confirmed by their uniform distribution on the substrate surface and the associated results of energy dispersive spectrometry (Supplementary Fig. 20). Notably, due to the universality of EDP, printing various nanomaterials simply follows the same process, eliminating the need for specialized design of nanomaterial dispersions and extra procedures. Particularly, the EDP is highly compatible to various nanomaterials without the need of additives, circumventing the meticulous regulation of rheological property of nanomaterial dispersions to meet the printing requirement, as encountered in inkjet/direct-ink-write (DIW) printing<sup>33</sup>.

In addition to single-component printing, EDP can also be implemented for constructing multifunctional composite films by using mixed nanomaterials or sequential printing. Fig. 3b showcases EDP-enabled composite films printed with mixed components of GO/PS and GO/MXene. In fact, various composite films can be printed from different mixed components of nanomaterials (Supplementary Figs. 21, 22). Notably, during mixed nanomaterials printing, there is a uniform distribution of titanium from MXene throughout the cross-section of the composite film, indicating a consistent distribution of both MXene and GO within the composite film (Supplementary Fig. 23). These EDP-enabled composite films can also be realized by a procedure of sequential printing. Fig. 3c demonstrates the fabrication of layered composite films through a multi-step printing strategy. In contrast to complex fabrication processes employed by other methods<sup>34</sup>, EDP simply requires to change the nanomaterial dispersion during the printing process in sequence. Using this method, a variety of multi-layer composite films, including CNT/GO/PS, GO/PS/CNT, and other configurations, can be achieved (Supplementary Figs. 24–26). Furthermore, by integrating two patterning strategies, EDP enables simultaneous macro-patterning and microstructural regulation,

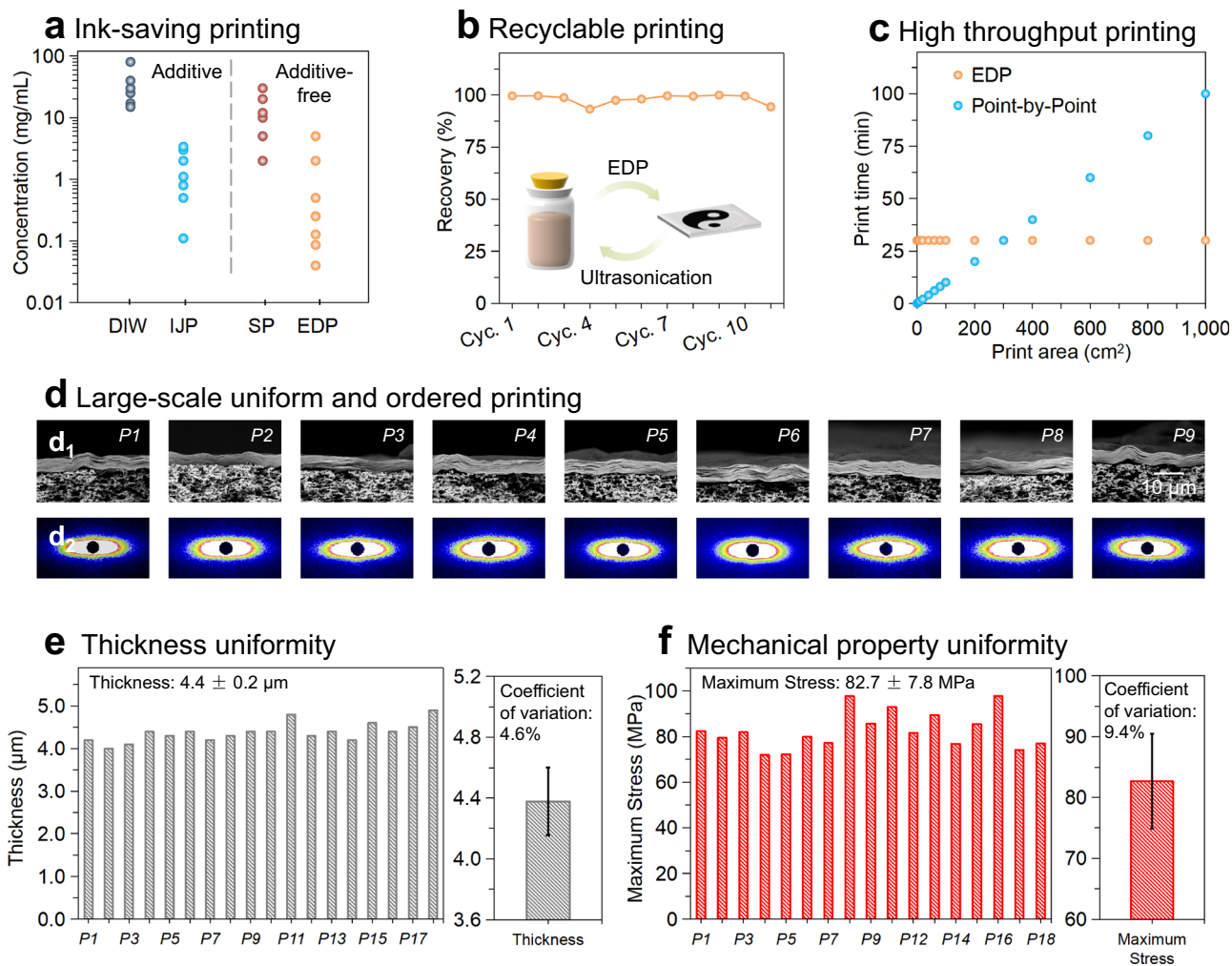


**Fig. 4 | Advantages of EDP.** **a** Comparison of GO concentration used in direct-ink-write (DIW), inkjet printing (IJP), Scraping printing (SP), and EDP. **b** Recyclable printing ability of EDP during a 10-cycle recyclable printing test. The inset is a schematic diagram of cyclic printing. **c** Comparison of necessary printing time with increasing printing area by EDP and point-by-point printing methods. **d** Large-scale

uniform order structure of EDP-enabled films: (d1) SEM images, (d2) Small-Angle X-ray Scattering (SAXS) images. **e** Thickness uniformity of EDP-enabled films. Data presented as mean  $\pm$  SD,  $n = 18$ . **f** Mechanical property uniformity of EDP-enabled films. Data presented as mean  $\pm$  SD,  $n = 18$ .

offering a broader range of options for material design and preparation (Supplementary Fig. 27).

#### Advantages of EDP over conventional printing strategies

The unique evaporation-driven process endows EDP with numerous advantages over traditional methods in nanomaterial printing. First, EDP is a material-saving printing technique (Fig. 4a) as it allows printing within a wide concentration range of ink, especially with a low concentration down to 0.04 mg/mL, which can minimize the nanomaterial dosage and is very beneficial for some expensive nanomaterials. The ink-saving nature originates from the evaporation-driven gathering effect of nanomaterials in dilute dispersion for forming a concentrated assembly. On the contrary, DIW and scraping printing need high ink concentration to ensure ink rheology. Moreover, both DIW and inkjet printing require corresponding additives to adjust the viscosity and other properties of the ink<sup>25</sup>. In contrast, additives are not necessary in EDP in most cases, significantly reducing the complexity of ink preparation. Second, EDP is a recyclable printing method as demonstrated in Fig. 4b (print PS, 300 nm). The printed microspheres can be easily re-dispersed in water through the application of ultrasonication. This re-dispersed solution can then be directly used for subsequent EDP printing to fabricate new films. To quantify the recovery potential of

this recycling process, the concentration of the dispersion was measured before EDP and after ultrasonication. A 10-cycle recovery test revealed an average recovery rate of 98.1%, showcasing the exceptional recyclability of the EDP process. In addition to the nanomaterials recovery, the evaporated water during EDP can also be recovered for further use. As illustrated in Supplementary Fig. 28, the evaporated water can be fully harvested using a water recovery system. Therefore, EDP represents a highly promising method for clean production with minimized material waste.

Furthermore, EDP is a high-throughput printing technology. Printing methods such as DIW and inkjet printing normally involve a dot or line scan mode and thus are time-intensive, which is detrimental to large-scale manufacturing demands. In contrast, EDP, as a layer-by-layer printing technology, has natural advantages in this regard. During EDP, nanomaterials are simultaneously and uniformly printed onto the entire surface of the substrate within the same time frame. As a result, the printing rate positively correlates to the printing area, and the printing time is determined by the printing thickness rather than the area. As shown in Fig. 4c, EDP demonstrates significant throughput advantages for large-area printing, despite taking longer for small-area printing compared to point-by-point methods. This layer-by-layer printing characteristic of EDP significantly reduces time cost for large-

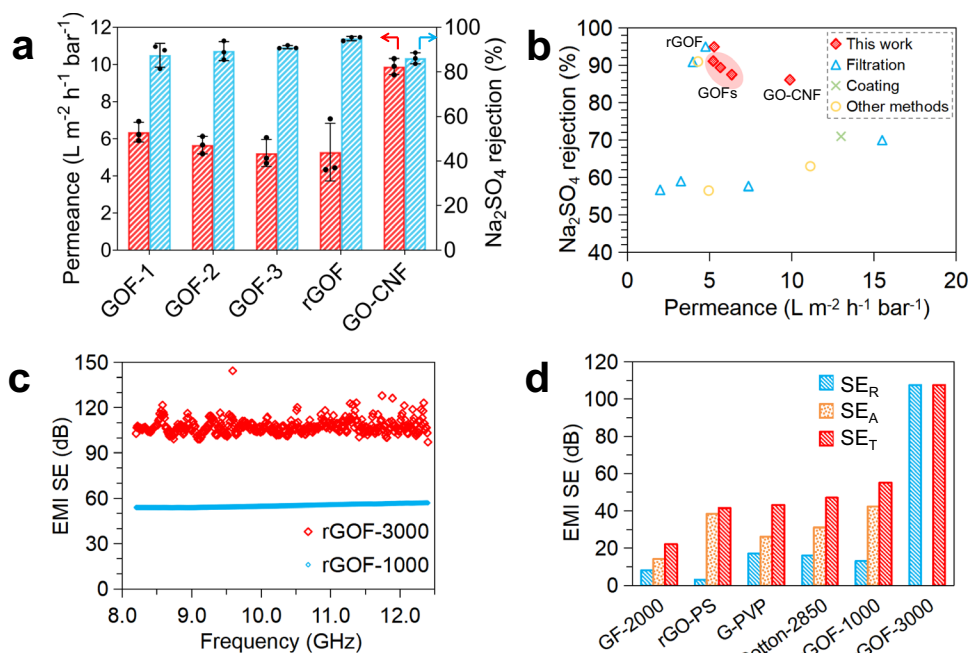


**Fig. 5 | Application potential of EDP-enabled films.** **a** Water permeance and  $\text{Na}_2\text{SO}_4$  rejection of EDP-enabled GO films (GOFs), reduced GO film (rGOF) and composite film of GO and CNF (GO-CNF). Data presented as mean  $\pm$  SD,  $n = 3$ . **b** Comparison of desalination performance of GOFs based on EDP and other methods: filtration<sup>40–44</sup>, coating<sup>45</sup> and other methods<sup>46–48</sup>. The raw data are given in

Supplementary Information Supplementary Table 4. **c** Electromagnetic interference shielding effect (EMI SE) of a series of rGOFs based on EDP. **d** Comparison of electromagnetic shielding performance among similar materials: GF-2000<sup>49</sup>, rGO-PS<sup>50</sup>, G-PVP<sup>51</sup>, Cotton-2850<sup>52</sup>. The raw data are given in Supplementary Information Supplementary Table 5.

scale printing. In addition, EDP demonstrates outstanding performance in the fabrication of ordered lamella films. The transmission electron microscopy images (Supplementary Fig. 29) and small-angle X-ray scattering data clearly reveal a distinct lamellar structure in the EDP-enabled GO films (Fig. 4d). Moreover, due to the uniform evaporation of water during the printing, this EDP-enabled large-scale film maintains excellent uniformity as illustrated in Fig. 4d, Supplementary Fig. 30. Comprehensive evaluations were conducted across various aspects such as the thickness (Figs. 4e,  $4.4 \pm 0.2 \mu\text{m}$ ), orientation degree (Supplementary Fig. 31a,  $0.86 \pm 0.02$ ), mechanical properties (Fig. 4f, maximum stress:  $82.7 \pm 7.8 \text{ MPa}$ ), electrical conductivity (Supplementary Fig. 31b,  $0.165 \pm 0.008 \text{ S/m}$ ), and thermal conductivity (Supplementary Fig. 31c,  $0.21 \pm 0.01 \text{ W/(m}\cdot\text{k)}$ ). These results are all maintained within a low coefficient of variation (CV), consolidating EDP's consistent quality in large-scale production and providing robust support for its scalability.

### Application potential of EDP-enabled films

Integrated films constructed from functional nanomaterials unlock the potential in various domains such as advanced membranes, electronic applications, and beyond<sup>35–37</sup>. As a proof of concept, we printed a series of GO-based films by EDP to assess their desalination performance, capitalizing on ultrafast water transport and exceptional molecule sieving abilities of lamellar GO nanochannels. Fig. 5a demonstrates the performance of printed GO films (GOF) in desalination ability using  $\text{Na}_2\text{SO}_4$  as a typical example. When GOF is reduced to rGOF, its rejection rate of  $\text{Na}_2\text{SO}_4$  has a significant increase, yet the water permeance decreases, due to the decreased interlayer spacing during reduction. With a remarkable rejection rate of 95.0%, significantly exceeding the performance of most previous GO/rGO-based membranes, the rGOF demonstrates exceptional separation capabilities. This high rejection rate is attributed to the regular arrangement of GO nanosheets and the defect-free nature of the printed film, highlighting the superior properties of EDP. Remarkably, leveraging the multi-material printing capacity of EDP, we further incorporated

nanomaterials such as cellulose nanofiber (CNF) to tune the interlayer spacing of GO to break the trade-off between rejection and permeance. As expected, GO-CNF films exhibit significantly enhanced water permeance due to the enlarged nanochannels for water permeation while maintaining a high rejection rate of 86.1%, attributed to the strong Donnan effect stemming from the negative charge of CNF. Fig. 5b further compares the performance of GOFs prepared by EDP with that in relevant literature, revealing that the printed GOFs outperform most counterparts prepared by traditional methods, demonstrating EDP as a simple yet efficient preparation method.

In addition to desalination applications, EDP is also capable of constructing high-performance electromagnetic shielding materials by virtue of a printed ordered lamellar structure as continuous conductive pathways. When EDP-enabled GOF is sequentially treated with ascorbic acid reduction, 1000 °C annealing (rGOF-1000), and 3000 °C annealing (rGOF-3000), its conductivity increased from 3.3 to 300 and 4600 S/cm. Consequently, their electromagnetic shielding effectiveness (EMI SE) increases from 0.17 to 55 and 107 (Fig. 5c). Compared to other similar materials, rGOF-1000 already surpasses them in total shielding effectiveness, with absorption shielding playing a dominant role (Fig. 5d). On the other hand, rGOF-3000 achieves a shielding effectiveness of around 107 dB, but almost entirely through reflection shielding, with negligible absorption shielding. This is because the 3000 °C high temperature fully graphitizes the graphene<sup>38,39</sup>, causing electromagnetic waves to be completely reflected at its surface, thus no absorption shielding can be detected. Furthermore, rGOF demonstrates excellent uniformity after thorough thermal annealing of the large-scale film (Supplementary Fig. 31d). Taken together, EDP can be used as a compelling manufacturing strategy to customize the composite, structure and function of nanomaterial-based films to advance their application potential.

### Discussion

In summary, we present a facile and generic evaporation-driven printing (EDP) of various nanomaterials on the surface of porous

substrates. Distinct from conventional strategies, EDP boasts universality, capable of processing nanomaterials of different species and dimensions, without being constrained by the physicochemical properties of the nanomaterial dispersion or the interfacial properties of the substrate. By being integrated into a roll-to-roll apparatus, the EDP allows for high-throughput roll-to-roll fabrication of large-scale functional films in a layer-by-layer printing manner. Moreover, EDP exhibits profound merits in multi-materials, recyclable, and material-saving printing, providing a simpler and more efficient material design strategy. EDP-enabled large-scale functional films hold the potential applications in water treatment, electromagnetic shielding and beyond. We envision that EDP is expected to further unleash the application potential of nanomaterials in various fields and accelerate the pace of large-scale application of nanomaterials-based films.

## Methods

### Materials

GO aqueous dispersion with high concentration (99%) was purchased from Hangzhou Gaoxi Technology Co., Ltd. GO powder (98%) was purchased from Shenzhen Qihang Technology Co., Ltd. Carboxylated multiwalled carbon nanotubes (CNT, 95%),  $\text{Ti}_3\text{AlC}_2$  (99%), LiF (99%), L-ascorbic acid (LAA, 99%) were purchased from Shanghai Macklin Biochemical Technology Co., Ltd. Blue fluorescent polystyrene microspheres (PS, 300 nm, 500 nm and 700 nm) purchased from Tianjin Beisile Chromatographic Technology Development Center. Sodium dodecyl sulfate (SDS) and polyvinyl pyrrolidone (PVP) were purchased from Shanghai Macklin Biochemical Technology Co., Ltd. Bacterial cellulose (BC) was purchased from Songhu Shenjian Technology Co., Ltd. Titanium dioxide ( $\text{TiO}_2$ , 30%) was purchased from Dashinou Nanotechnology (Changzhou) Co., Ltd. Aluminum oxide ( $\text{Al}_2\text{O}_3$ , 40%) was purchased from Shenzhen Crystal Material Chemical Co., Ltd. Montmorillonite (MMT) was purchased from Shandong Yusuo Chemical Technology Co., Ltd. Kaolin (KL) was purchased from Tianjin Juhengda Chemical Co., Ltd. Polyether sulfone (PES) microfiltration membranes, CN-CA (CN-CA) microfiltration membranes, polypropylene (PP) microfiltration membranes, polytetrafluoroethylene (PTFE) microfiltration membranes, regenerated cellulose (RCE) microfiltration membranes and mixed cellulose ester (MCE) microfiltration membranes were purchased from Haiyan New Oriental Plastics Technology Co., Ltd, Haining Yanguan Chuangwei Filter Equipment Factory, Haining Yibo Filter Equipment Factory. Polyethersulfone (PES) ultrafiltration (UF) membrane was provided by Vontron Technology Co., Ltd. (China).

### Experimental procedure of evaporation-driven printing (EDP)

The general experimental steps for EDP are as follows (taking a 1.0 mg/mL GO dispersion as an example of ink). In a typical experiment, 25 mg of GO were added to 25 mL of deionized water. The dispersion was stirred and sonicated for 30 min to ensure even dispersion of the GO. After thorough ultrasonic treatment, the GO dispersion was transferred to a petri dish and heated in a water bath at 80 °C for 10 min. A substrate was then placed at the air-liquid interface of the dispersion, and the water bath heating was continued for an additional 30 min. Afterwards, the substrate was carefully transferred onto a flat surface with the printed GO side facing up and allowed to dry at room temperature for 6 h.

Notes: Paste-like GO is prepared to the desired concentration through dilution. The dispersion is preheated to remove the dissolved gas to minimize the occurrence of defects during EDP. A small amount of surfactant (SDS or PVP) is required to aid in the dispersion of CNTs. MXene is prepared from  $\text{Ti}_3\text{AlC}_2$ . For other materials, uniform dispersions of the desired concentration are prepared according to the actual conditions of the materials. Most porous organic membranes can float on the dispersion. Glass fiber membranes and alumina membranes need to be fixed at the air-liquid interface using clips or

other suitable methods. Additionally, the printing temperature, time, and concentration are adjusted according to specific printing requirements.

### Verification of pressure difference with/without evaporation

The GO is printed onto two PES substrate membranes, and they are allowed to dry at room temperature for one hour to facilitate partial evaporation of water from the printed structures. Two containers filled with deionised water were placed into a transparent water bath set at 75 °C, and they were preheated for 20 min. The PES substrates, with the printed GO side facing the aqueous phase, are positioned at the air-liquid interface of each container. The water bath conditions are maintained by leaving one container open and sealing the other. The changes in the printed GO are observed and photographed over time.

### Patterned printing

**Front-masking.** The general experimental steps for the Front-masking strategy in EDP (taking GO as an example) are as follows. The patterned adhesive tape is applied onto the PES substrate and set aside for later use. The 1 mg/mL GO dispersion solution, serving as the ink, is prepared and preheated in an 80 °C water bath for 10 min. The PES substrate is then placed at the air-liquid interface of the GO ink, with the patterned adhesive tape facing the liquid phase side. After maintaining the water bath at 80 °C for 30 min, the substrate is transferred to a flat surface, with the printed GO facing upwards. It is allowed to dry at room temperature for 6 h, resulting in a patterned printed GO film.

**Back-masking.** The general experimental steps for the Back-masking strategy in EDP patterned printing are similar to those of the Front-masking strategy. The key difference lies in the position of the patterned tape on the PES substrate when it is placed at the air-liquid interface of the GO ink. For the Back-masking strategy, the patterned tape faces the gas phase side, with no direct contact with the GO ink.

### Printing of composite films

The general process of printing composite films by EDP is outlined below, with GO/MXene as an illustrative example. A mixed solution of GO and MXene is used as the printing ink. The concentration ratio of GO to MXene is adjusted to 5:1 and 1:5, with a total concentration of 3.0 mg/mL. This solution is then subjected to ultrasonic treatment for 30 min at 20 °C to ensure uniform dispersion. Subsequently, the solution is preheated in an 80 °C water bath for 10 min, and a PES substrate is floated above the GO/MXene ink. This setup is maintained in the water bath for an additional 30 min. Following this, the substrate is transferred and allowed to dry for 6 h, resulting in the formation of a GO/MXene composite film. The same method is applied to the preparation of GO/CNT and GO/PS composite films, with adjustments made to the ink composition according to the specific design requirements.

### Printing of layered composite films

The general experimental steps for printing layered composite films by EDP are as follows (taking the GO/CNT/PS layered composite film as an example). Firstly, GO, CNT, and PS dispersions are prepared uniformly in three separate beakers and placed in an 80 °C water bath for standby use. Secondly, the PES substrate is placed at the air-liquid interface of the GO dispersion, and the water bath is maintained at 80 °C for 30 min. Then, the PES substrate with printed GO is transferred to the surface of the CNT dispersion, and the water bath is maintained at 80 °C for another 30 min to form a GO/CNT layered structure. Thirdly, the substrate is transferred to the air-liquid interface of the PS dispersion, and the water bath is maintained at 80 °C for another 30 min to form a GO/CNT/PS layered structure. After the substrate is transferred to a dry surface, it is allowed to dry at room temperature for 6 h to obtain the GO/CNT/PS layered composite film. The composition of

each layer in the layered composite film can be controlled by adjusting the inks, and the thickness can be adjusted according to the printing time. To prepare layered composite films with more layers, simply repeat the above steps.

## Data availability

All data supporting the findings of this study are available in the manuscript and its Supplementary Information. Source data are provided with this paper. Other related raw data are fully and freely available from the corresponding authors. Source data are provided with this paper.

## References

- Liu, Y. N., Coppens, M. O. & Jiang, Z. Y. Mixed-dimensional membranes: chemistry and structure-property relationships. *Chem. Soc. Rev.* **50**, 11747–11765 (2021).
- Mohammadi, A. V., Rosen, J. & Gogotsi, Y. The world of two-dimensional carbides and nitrides (MXenes). *Science* **372**, 1165–1166 (2021).
- Sun, M. & Li, J. H. Graphene oxide membranes: functional structures, preparation and environmental applications. *Nano Today* **20**, 121–137 (2018).
- Karahan, H. E. et al. MXene materials for designing advanced separation membranes. *Adv. Mater.* **32**, 23 (2020).
- Wang, S. F. et al. Two-dimensional nanochannel membranes for molecular and ionic separations. *Chem. Soc. Rev.* **49**, 1071–1089 (2020).
- Chen, L. et al. Ion sieving in graphene oxide membranes via cationic control of interlayer spacing. *Nature* **550**, 415–418 (2017).
- Kumar, A. & Mandal, D. 2D-pyroelectric materials for waste thermal energy harvesting and beyond. *Adv. Energy Mater.* <https://doi.org/10.1002/aenm.202403319> (2024).
- Lin, W. H. et al. Novel ultrastable 2D MOF/MXene nanofluidic membrane with ultralow resistance for highly efficient osmotic power harvesting. *Nano Energy* **128**, 9 (2024).
- Pan, X. Y. et al. 2D MXenes polar catalysts for multi-renewable energy harvesting applications. *Nat. Commun.* **14**, 11 (2023).
- Hu, J. K. et al. 2D graphene oxide: a versatile thermo-optic material. *Adv. Funct. Mater.* <https://doi.org/10.1002/adfm.202406799> (2024).
- Li, K. R. et al. Biomimetic MXene textures with enhanced light-to-heat conversion for solar steam generation and wearable thermal management. *Adv. Energy Mater.* **9**, 14 (2019).
- Lee, G. S. et al. 2D materials beyond post-Al era: smart fibers, soft robotics, and single atom catalysts. *Adv. Mater.* **36**, 40 (2024).
- Zhao, Y. & Lin, L. Graphene, beyond lab benches. *Science* **386**, 144–146 (2024).
- Kadja, G. T. M. et al. Advances and challenges in the development of nanosheet membranes. *Rev. Chem. Eng.* **39**, 631–668 (2023).
- Huang, H. B. et al. Ultrafast viscous water flow through nanostrand-channelled graphene oxide membranes. *Nat. Commun.* **4**, 9 (2013).
- Nair, R. R., Wu, H. A., Jayaram, P. N., Grigorieva, I. V. & Geim, A. K. Unimpeded permeation of water through helium-leak-tight graphene-based membranes. *Science* **335**, 442–444 (2012).
- Qian, W. et al. Scalable assembly of high-quality graphene films via electrostatic-repulsion aligning. *Adv. Mater.* **34**, 8 (2022).
- Dikin, D. A. et al. Preparation and characterization of graphene oxide paper. *Nature* **448**, 457–460 (2007).
- Chai, Z. M., Korkmaz, A., Yilmaz, C. & Busnaina, A. A. High-rate printing of micro/nanoscale patterns using interfacial convective assembly. *Adv. Mater.* **32**, 8 (2020).
- Chen, C. et al. Self-assembled free-standing graphite oxide membrane. *Adv. Mater.* **21**, 3007–3011 (2009).
- Shim, J. et al. Two-minute assembly of pristine large-area graphene-based films. *Nano Lett.* **14**, 1388–1393 (2014).
- Kronenfeld, J. M., Rother, L., Saccone, M. A., Dulay, M. T. & DeSimone, J. M. Roll-to-roll, high-resolution 3D printing of shape-specific particles. *Nature* **627**, 12 (2024).
- Deleka, S. S., Laurila, M. M., Mäntysalo, M. & Li, J. T. Drying-mediated self-assembly of graphene for inkjet printing of high-rate micro-supercapacitors. *Nano-Micro Lett.* **12**, 14 (2020).
- Zeng, M. X. et al. High-throughput printing of combinatorial materials from aerosols. *Nature* **617**, 292 (2023).
- Hu, G. H. et al. Functional inks and printing of two-dimensional materials. *Chem. Soc. Rev.* **47**, 3265–3300 (2018).
- Saadi, M. et al. Direct Ink writing: a 3D printing technology for diverse materials. *Adv. Mater.* **34**, 57 (2022).
- Tran, T. S., Dutta, N. K. & Choudhury, N. R. Graphene inks for printed flexible electronics: graphene dispersions, ink formulations, printing techniques and applications. *Adv. Colloid Interface Sci.* **261**, 41–61 (2018).
- Xue, G. B. et al. Water-evaporation-induced electricity with nanostructured carbon materials. *Nat. Nanotechnol.* **12**, 317–321 (2017).
- Zhao, C. et al. Layered nanocomposites by shear-flow-induced alignment of nanosheets. *Nature* **580**, 210–215 (2020).
- Chouhan, A., Mungse, H. P. & Khatri, O. P. Surface chemistry of graphene and graphene oxide: a versatile route for their dispersion and tribological applications. *Adv. Colloid Interface Sci.* **283**, 28 (2020).
- Evans, A. A., Cheung, E., Nyberg, K. D. & Rowat, A. C. Wrinkling of milk skin is mediated by evaporation. *Soft Matter* **13**, 1056–1062 (2017).
- Xu, G.-C. et al. Supergravity-steered generic manufacturing of nanosheets-embedded nanocomposite hydrogel with highly oriented, heterogeneous architecture. *Adv. Mater.* **36**, 2400075 (2024).
- Shahbazi, M. et al. Dispersion strategies of nanomaterials in polymeric inks for efficient 3D printing of soft and smart 3D structures: a systematic review. *Adv. Colloid Interface Sci.* **333**, 38 (2024).
- Huang, G. W., Feng, Q. P., Xiao, H. M., Li, N. & Fu, S. Y. Rapid laser printing of paper-based multilayer circuits. *ACS Nano* **10**, 8895–8903 (2016).
- Pomerantseva, E., Bonaccorso, F., Feng, X. L., Cui, Y. & Gogotsi, Y. Energy storage: the future enabled by nanomaterials. *Science* **366**, 969–96 (2019).
- Cho, K. W. et al. Soft bioelectronics based on nanomaterials. *Chem. Rev.* **122**, 5068–5143 (2022).
- Kelly, A. G. et al. All-printed thin-film transistors from networks of liquid-exfoliated nanosheets. *Science* **356**, 69–72 (2017).
- Li, T. et al. Thermoelectric properties and performance of flexible reduced graphene oxide films up to 3000 K. *Nat. Energy* **3**, 148–156 (2018).
- Akbari, A. et al. Highly ordered and dense thermally conductive graphitic films from a graphene oxide/reduced graphene oxide mixture. *Matter* **2**, 1198–1206 (2020).
- Wang, J. Q. et al. Graphene oxide as an effective barrier on a porous nanofibrous membrane for water treatment. *ACS Appl. Mater. Interfaces* **8**, 6211–6218 (2016).
- Han, Y., Xu, Z. & Gao, C. Ultrathin graphene nanofiltration membrane for water purification. *Adv. Funct. Mater.* **23**, 3693–3700 (2013).
- Han, Y., Jiang, Y. Q. & Gao, C. High-flux graphene oxide nanofiltration membrane intercalated by carbon nanotubes. *ACS Appl. Mater. Interfaces* **7**, 8147–8155 (2015).
- Li, Y. et al. Mild annealing reduced graphene oxide membrane for nanofiltration. *J. Membr. Sci.* **601**, 7 (2020).
- Zhang, M. C., Sun, J. J., Mao, Y. Y., Liu, G. P. & Jin, W. Q. Effect of substrate on formation and nanofiltration performance of graphene oxide membranes. *J. Membr. Sci.* **574**, 196–204 (2019).

45. Kim, J. H. et al. Scalable fabrication of deoxygenated graphene oxide nanofiltration membrane by continuous slot-die coating. *J. Membr. Sci.* **612**, 8 (2020).
46. Chen, L. et al. High-performance graphene oxide nanofiltration membrane prepared by electrospraying for wastewater purification. *Carbon* **130**, 487–494 (2018).
47. Chen, L. et al. A large-area free-standing graphene oxide multilayer membrane with high stability for nanofiltration applications. *Chem. Eng. J.* **345**, 536–544 (2018).
48. Du, Y. et al. Ultra-thin graphene oxide films via the contra-diffusion method: Fast fabrication for ion rejection. *J. Membr. Sci.* **595**, 7 (2020).
49. Shen, B., Zhai, W. T. & Zheng, W. G. Ultrathin flexible graphene film: an excellent thermal conducting material with efficient EMI shielding. *Adv. Funct. Mater.* **24**, 4542–4548 (2014).
50. Yan, D. X. et al. Structured reduced graphene oxide/polymer composites for ultra-efficient electromagnetic interference shielding. *Adv. Funct. Mater.* **25**, 559–566 (2015).
51. Wei, Q. W. et al. Superhigh electromagnetic interference shielding of ultrathin aligned pristine graphene nanosheets film. *Adv. Mater.* **32**, 9 (2020).
52. Ma, X. H. et al. Carbon composite networks with ultrathin skin layers of graphene film for exceptional electromagnetic interference shielding. *ACS Appl. Mater. Interfaces* **10**, 38255–38263 (2018).

## Acknowledgments

This work is financially supported by the Natural Science Foundation of Zhejiang Province (Grant no. LZ24E030001 and LD22E030001), the National Natural Science Foundation of China (Grant no. 21805022, 22135006, 22375174, and 52203281), and the Fundamental Research Funds for the Central Universities (Grant no. 226-2024-00027 and Grant no. 226-2025-00011). Dr Chao Zhang acknowledges gratefully the research startup package from Zhejiang University.

## Author contributions

X.X. (corresponding author) conceived the initial idea and wrote the initial manuscript. C.Z. (corresponding author) and Z.K.X. (corresponding author) conceived the idea for the project and revised the manuscript. Y.W.L. and J.H.X. designed the experiments and performed the majority of them. Z.H.L. conducted experiments for mechanism verification. H.Y.O. carried out experiments for Roll-to-Roll printing. H.F.Z. conducted experiments for patterned printing. C.Z. discussed the initial idea and provided constructive input. C.W.G. and X.B.H. conducted the

derivation of the mechanism. H.C.Y. participated in the discussion and offered constructive feedback.

## Competing interests

The authors declare no competing interests.

## Additional information

**Supplementary information** The online version contains supplementary material available at <https://doi.org/10.1038/s41467-025-66455-8>.

**Correspondence** and requests for materials should be addressed to Xu Xiang, Chao Zhang or Zhi-Kang Xu.

**Peer review information** *Nature Communications* thanks the anonymous reviewers for their contribution to the peer review of this work. A peer review file is available.

**Reprints and permissions information** is available at <http://www.nature.com/reprints>

**Publisher's note** Springer Nature remains neutral with regard to jurisdictional claims in published maps and institutional affiliations.

**Open Access** This article is licensed under a Creative Commons Attribution-NonCommercial-NoDerivatives 4.0 International License, which permits any non-commercial use, sharing, distribution and reproduction in any medium or format, as long as you give appropriate credit to the original author(s) and the source, provide a link to the Creative Commons licence, and indicate if you modified the licensed material. You do not have permission under this licence to share adapted material derived from this article or parts of it. The images or other third party material in this article are included in the article's Creative Commons licence, unless indicated otherwise in a credit line to the material. If material is not included in the article's Creative Commons licence and your intended use is not permitted by statutory regulation or exceeds the permitted use, you will need to obtain permission directly from the copyright holder. To view a copy of this licence, visit <http://creativecommons.org/licenses/by-nc-nd/4.0/>.

© The Author(s) 2025